Study of the Li/Li3N electrode in an organic electrolyte.

J. Thévenin, R.H. Muller

Lawrence Berkeley National Laboratory
Recent Work

Title
STUDY OF THE Li/Li3N ELECTRODE IN AN ORGANIC ELECTROLYTE

Permalink
https://escholarship.org/uc/item/4ng5n8bd

Authors
Thevenin, J.G.
Muller, R.H.

Publication Date
1986

Lawrence Berkeley Laboratory
UNIVERSITY OF CALIFORNIA

Materials & Chemical Sciences Division

STUDY OF THE Li/Li$_3$N ELECTRODE IN AN ORGANIC ELECTROLYTE

J.G. Thevenin and R.H. Muller

January 1986

DISCLAIMER

STUDY OF THE Li/Li$_3$N ELECTRODE
IN AN ORGANIC ELECTROLYTE

J.G. Thevenin* and R.H. Muller

Lawrence Berkeley Laboratory
University of California
Berkeley, CA 94720

January 1986

*Permanent Address: Universite Pierre et Marie Curie, T22-5E,
F75230 Paris, France.

ABSTRACT

Lithium nitride has been studied as a possible solid-electrolyte interphase between the lithium electrode and an organic electrolyte. The Li/Li_3N electrode has been obtained by exposing lithium to a pure nitrogen atmosphere at ambient temperature. This procedure is found to lead to the formation of a porous lithium nitride film, resulting from a decrease in the molar volume during the reaction. The impedance behavior of the Li/Li_3N electrode can be interpreted by a porous-film model deduced from a transmission-line model. The slow filling of the micropores of the film and reaction of lithium with the electrolyte at the pore bases are responsible for changes of impedance and open-circuit potential with time and under cycling.

INTRODUCTION

When a lithium electrode is stored in an organic electrolyte, a surface layer is usually formed, due to the decomposition products of the solvent and salt in the presence of lithium.[1,2] This surface layer inhibits the successful cycling of the lithium electrode. One possible way to limit the formation of the surface layer is to place an ionic conductor that is less reactive than lithium between the electrode and the electrolyte. A survey of the literature suggests that lithium nitride may be an excellent candidate for this purpose because it is a solid electrolyte with a high ionic conductivity.[3-5] The use of a lithium nitride film to protect lithium against chemical corrosion in organic electrolytes has been proposed earlier by Muller and Schwager.[6]

The purpose of this paper is to analyze the morphological and kinetic properties of lithium nitride, formed by exposure of lithium at ambient temperature to a nitrogen atmosphere, as a possible interphase between lithium and a propylene carbonate-based electrolyte.

THEORETICAL

The impedance behavior of the metal/film/solution system is primarily determined by the morphological and kinetic properties of the film. Because this film between the metal and the solution is polycrystalline, it can be compact or porous. The models described in detail below take into account the structure of the film for an analysis of the equivalent circuit of the system. The impedance spectrum is deduced under the assumption that only ionic conduction is involved in the film.

1. Model of a Compact Film

For a polycrystalline material, as shown in Fig. 1a, the transcrystalline and intercrystalline conduction processes can be represented by different equivalent circuits.[5] The transcrystalline resistance R_t and the capacitance C_t are related to the conductivity inside each particle, while the intercrystalline resistance R_i and the capacitance C_i are related to the conductivity between two adjacent particles. The resulting circuit is a series of R_t/C_t and R_i/C_i circuits as shown in Fig. 1b. A large dispersion of time constants for the intercrystalline conduction is due to different causes among them the random orientation of anisotropic particles. The impedance of each circuit is defined by the Cole-Cole formula,[7] and the total impedance for a radial frequency ω is given by:

$$Z(\omega) = \frac{R_t}{1 + (j\omega R_t C_t)^{(1-\alpha_t)}} + \frac{R_i}{1 + (j\omega R_i C_i)^{(1-\alpha_i)}} \qquad (1)$$

where j is the imaginary unit and α_t and α_i are the depression parameters corresponding to the dispersion of the time constants in the transcrystalline and intercrystalline impedances, respectively. The resulting impedance diagram in the complex plane for the Li/Li_3N electrode consists of two depressed semicircles, as shown schematically in Fig. 1c. The transcrystalline impedance can be detected only in the very high-frequency range, while the intercrystalline impedance is found in the intermediate- and low-frequency range.

2. Model of a Porous Film

For a metal electrode covered by a porous material, the impedance behavior can be studied by a transmission-line model,[8] provided that the finite thickness of the porous material and the impedance of the metal electrode are recognized.[9] The porous film of thickness L, illustrated in Fig. 2a, is assumed to have a homogeneous structure with almost parallel and cylindrical pores and constant composition along the pore wall. Thus, the equivalent electrical circuit for a single pore is determined by the properties of the liquid and solid phases, as shown in Fig. 2b. For the case of a lithium nitride film on a lithium electrode, the different elementary impedances can be described as follows: The liquid phase filling the pores is the organic electrolyte with an average liquid-phase resistance per unit pore length of R_1/L. The solid phase is the lithium nitride film with an average solid-phase impedance per unit pore length of Z_s/L. Under these conditions, the impedance behavior of the Li/Li_3N electrode is also determined by two

additional impedances. The impedance occurring on the pore base Z_b, independent of the pore length, is the impedance of the Li/liquid-electrolyte interface. The admittance occurring at the pore wall, $1/Z_p L$, per unit pore length, is the impedance of the Li_3N/liquid-electrolyte interface.

The total equivalent circuit is given in Fig. 2b and the total impedance, Z, resulting from n straight parallel, cylindrical pores defined by the transmission-line model,[9] is defined as follows:

$$Z = \frac{1}{n} \left\{ \frac{Z_s \cdot R_1}{Z_s + R_1} + \frac{2\gamma^{1/2} Z_s R_1 + \gamma^{1/2} (Z_s^2 + R_1^2) C + \delta R_1^2 S}{L\gamma^{1/2} (Z_s + R_1)(\gamma^{1/2} S + \delta C)} \right\} \tag{2}$$

where
$$\gamma = \frac{Z_s + R_1}{Z_p L^2} \qquad \delta = \frac{Z_s + R_1}{Z_b L} \tag{3}$$

and
$$C = \cosh(\gamma^{1/2} L) \qquad S = \sinh(\gamma^{1/2} L) \tag{4}$$

Simple modifications allow the equation of the total impedance to be extended to a three-dimensional system, by defining the different surface areas covered by the solid and liquid phases.[9] For example, if $(1-\Theta)$ is the fraction of the area occupied by pores, then the average areas of the pore base and solid base are defined by $(1-\Theta)/n$ and Θ/n, respectively. Thus, R_1 and Z_s, the liquid-phase and solid-phase

impedances, can be determined as a function of their respective specific quantities RL and ZS defined for planar systems:

$$R_1/L = RL \ n/(1-\Theta)L \tag{5}$$

$$Z_s/L = ZS \ n/\Theta L \tag{6}$$

On the other hand, knowledge of the average dimensions of the pores, especially the surface area of the pore wall of length L, permits one to determine Z_b and Z_p as a function of their respective specific quantities defined for planar systems ZB and ZP:

$$Z_b = ZB \ n/(1-\Theta) \tag{7}$$

$$Z_pL = ZP \ n^{1/2}/2 \ \pi^{1/2}(1-\Theta)^{1/2} \tag{8}$$

Under these assumptions, for a given set of parameters, the impedance behavior of the metal electrode covered by a porous material can be analyzed by computer simulation. For a polycrystalline material such as lithium nitride, which is characterized by two types of impedance, the computer-generated impedance diagram in the complex plane consists of two depressed semicircles over the whole frequency range, as shown schematically in Fig. 2c. The apparent transcrystalline and intercrystalline impedances depend on the assumptions made for the relative importance of the pore-base and

pore-wall impedances compared to the liquid-phase and solid-phase

impedances.

EXPERIMENTAL

1. Electrolyte

A molar solution of lithium perchlorate in propylene carbonate has

been prepared by use of propylene carbonate (Burdick and Jackson Lab)

which was dehydrated over molecular sieves for about two weeks and

lithium perchlorate (Smith Chem. Co.), dessicated near its melting

point (240 $^\circ$C) for one day under the vacuum of a mechanical pump.

2. Li/Li$_3$N Electrode

Lithium nitride was prepared by the reaction of lithium and

nitrogen at room temperature. The reaction was carried out in an

inflated PVC plastic bag which had been repeatedly filled with

high-purity nitrogen. The same results have been obtained in pure

nitrogen and nitrogen diluted with helium at different ratios. Film

growth was initiated by cutting, under nitrogen, a lithium cylinder on

a cross-section with a stainless steel blade. The oxygen and water

content in the nitrogen used is estimated to be well below 10 ppm. The

resulting film is not protective against further reaction with nitrogen

and a complete conversion of lithium to lithium nitride occurs after

extended exposure. The growth generally began with an iridescent film

on most of the lithium surface. A continuous red-black film developed

starting from the circumference of the lithium disc, and spreading over the entire surface after about 20 minutes of exposure to nitrogen. Without exposure to air, the nitride- covered lithium electrode was transferred to the helium-filled glove box, where it was inserted in the electrolytic cell. Difficulties were encountered in reproducing the growth of this film; the reasons for these difficulties are not well understood. The speed of cutting and the roughness of the resulting surface seem to be important for the nucleation and growth of the lithium nitride layer. The present procedure was found to result in a more uniform film growth than a previously used, more cumbersome method, in which the lithium was cut in the recirculated He atmosphere of an inert atmosphere glove box and transferred to a nitrogen-filled bag inside the glove box. In air, a more rapidly-formed oxide layer largely prevents nitride formation.

3. Experimental Set-up

The electrolytic cell of 30 cc liquid volume was made of polypropylene. It was equipped with two opposing openings for the polypropylene electrode holders and an extrusion compartment for the lithium reference electrode. The working electrode was the cross-section of a lithium cylinder 0.2 cm in diameter and 0.5 cm thick covered by a lithium nitride film about 0.01 cm thick. The reference electrode was the cross-section of a lithium cylinder 0.2 cm in diameter. The counter electrode was a lithium disc 2 cm in diameter and 0.1 cm thick.

The electrode-impedance data have been obtained by the Lissajous-figure technique at the open-circuit potential of the Li/Li_3N electrode. The equipment includes an oscillator (Hewlett Packard, Model 3310A), which drives a potentiostat-galvanostat (Princeton Applied Research, Model 173) in the galvanostatic mode. The oscillating current and voltage were measured by two external differential preamplifiers (Princeton Applied Research, Model 113). Current versus voltage was displayed on a storage oscilloscope (Tektronix, Model 5111). The alternating-current density was about 0.05 mA/cm^2, which provided a linear response, as required for valid electrode-impedance measurements. Measurements were also conducted over the frequency range of 10^4 to 10^{-1} Hz on a model circuit with resistance and capacitance similar to those of the electrode under study to ensure that the equipment was in proper working condition. The high-frequency limit was chosen to avoid any artifacts caused by the impedance of the reference electrode, while the low-frequency limit was necessary to obtain quick measurements independent of the change of the electrode impedance with the time of immersion of the electrode in the solution.

RESULTS AND DISCUSSION

1. Morphological Properties of the Li/Li_3N Electrode

Scanning electron microscopy of the surface of the lithium nitride film shows that the ridges on the lithium electrode resulting from the

cutting were preserved during the formation of the thin lithium nitride film, (Fig. 3), thus wrongly suggesting formation of a compact film. After 20 min. of exposure of lithium to nitrogen, the minimum thickness in the center of the film was about 0.01 cm, while the maximum thickness, at the circumference of the disc was higher than 0.1 cm, as shown in Fig. 4. A lithium nitride film of 0.5 cm thickness, formed after one hour of exposure of lithium to nitrogen, gave evidence of cracks and holes on its surface, as shown in Fig. 5. They are clues to the porosity of the film caused by the decrease of the molar volume during the conversion of lithium to lithium nitride. As shown below most of the pores are, however, too small to be visible by scanning electron microscopy.

Mercury porosimetry confirmed that the preparation procedure used to form lithium nitride results in a porous film. The cumulative volume of intruded mercury as a function of applied pressure, shown in Fig. 6, for 0.7 cm thick lithium nitride films shows changes of slope at about 5×10^2 and 3×10^3 Kg/cm^2 indicating the occurrence of two classes of pore radii of about 150 and 25 Å, respectively. The maximum pressure used for the measurement (up to 4×10^3 Kg/cm^2) was, however, not sufficient to fill all the voids in the samples. The differential pore-volume density as a function of the pore radius, shown in Fig. 7, presents a slight maximum in the 100-200 Å pore-radius range and a sharp one in the pore-radius range below 25 Å. The differential pore-surface and pore-length densities, showing only a peak for small pore radii, allows one to assume that the porosity of thick lithium

nitride films is essentially due to interparticle voids.

The density of the lithium nitride samples has also been deduced from the mercury intrusion studies. Taking into account the apparent volume and weight of the samples, the density of porous lithium nitride is evaluated to be 0.97 g/cm^3. By measuring the weight and volume of the intruded mercury into the micropores, the density of the equivalent compact lithium nitride is evaluated to be 1.22 g/cm^3, in good agreement with the density (1.29 g/cm^3) which has been reported for lithium nitride single crystals. (See Table 1)

2. Potential Behavior of the Li/Li$_3$N Electrode

The value of the open-circuit potential of a 1 cm thick Li$_3$N electrode is about 0.36 V measured versus the Li electrode. This value is close to the thermodynamic potential (E_0 = 0.44 V) which can be extrapolated for ambient temperature from the energy of formation of lithium nitride.[12,13] There is no evidence of chemical reaction between lithium nitride and the propylene carbonate-based electrolyte. Even during an anodic polarization up to 1 V versus lithium, the decomposition of lithium nitride has not been observed despite its low thermodynamic potential.

The open-circuit potential of the Li/Li$_3$N electrode formed with a thin Li$_3$N film depends on its preparation procedure and polarization conditions. For example, as shown in Fig. 8, the potential increases with the thickness of the Li$_3$N film, and decreases with the immersion time in the solution. An electrode, formed by 20 min. of exposure of

lithium to nitrogen had a potential of about 0.2 V just after

immersion; this open-circuit potential was reduced to a stable value of

0.01 V after one day of immersion in the solution. The open-circuit

potential of the Li/Li$_3$N electrode also depends on its polarization

history, as shown in Figs. 9 and 10. A cathodic deposition or an

anodic dissolution with low current and charge densities led to a

decrease of the electrode potential measured after the interruption of

polarization. This potential behavior can be attributed to a slow

filling of the micropores of the lithium nitride film leading to a

direct contact of the organic electrolyte with the lithium metal.

3. Impedance Behavior of the Li/Li$_3$N Electrode

The analysis of impedance diagrams in the complex plane, as shown

in Fig. 11, suggests the occurrence of two types of impedances as

expected for the compact-film model. The total resistance can be

separated into the transcrystalline resistance R_t (high-frequency

range), and the intercrystalline resistance R_i (low-frequency range).

The fact that the semicircles have their centers far below the real

axis, with a high depression parameter can be attributed to a large

dispersion in the time constants related to the dielectric and

resistive properties of the polycrystalline lithium nitride film. For

an electrode formed by 20 min. of exposure of lithium to nitrogen, the

total resistance is about 200 Ω cm^2 immediately after immersion in the

electrolyte. Taking into account a minimum thickness of 0.01 cm for

the lithium nitride film, an apparent transcrystalline conductivity σ_t of

$3 \times 10^{-4} \Omega^{-1} cm^{-1}$, and an apparent intercrystalline conductivity σ_i of 6 $\times 10^{-5} \Omega^{-1} cm^{-1}$ can be deduced. These values, are of the same order as those observed for lithium nitride sinters.[5] (See Table 1)

The study of the impedance behavior of the Li/Li_3N electrode as a function of different parameters, such as immersion time and polarization conditions, shown in Figs. 12-14, further demonstrates that the lithium nitride film cannot be considered as a compact film. As the pores are progressively filled by the electrolyte, transcrystalline and intercrystalline impedances can no longer be separated and the high-frequency semicircle attributed to the transcrystalline impedance (shown by dashed lines) disappears. Figure 12 shows the change of the impedance diagrams with the immersion time in the organic electrolyte up to 48 hours. The conduction impedance is reduced in the intermediate-frequency range, and a diffusion impedance can be detected in the low-frequency range. Figures 13 and 14 show that, for different charge and current densities, a cathodic polarization as well as an anodic polarization leads to a decrease in the conduction impedance. The diffusion impedance which appears only for cathodic polarization and increases with the charge density is probably due to the diffusion of lithium ions along the pores. Besides, a single deposition/dissolution cycle, as shown in Fig. 15, leads to a decrease in the electrode impedance, an effect observed for different current and charge densities. For repeated cycles, during the fifth cycle for example, the cathodic polarization leads to a low impedance, while the subsequent anodic polarization leads to high impedance, as

shown in Fig. 16. This behavior seems to be related to the formation of a lithium deposit on top of the lithium nitride film. This deposit can react with the solution to form a surface layer.

The porous-film model seems to be much more useful than the compact-film model for understanding the origin of the impedance behavior of the Li/Li_3N electrode. In principle, all the information about the porous system can be derived by fitting the curve of its impedance spectrum to the general equation of the total impedance. In practice, however, when considering the number of parameters (more than 7 for the analysis of a 3-dimensional system), the curve-fitting technique cannot be accurate enough and unique. Thus, at this time it is only possible to show that the porous-film model is reasonable for describing the Li/Li_3N electrode. The effect of porosity of lithium nitride on theoretically predicted impedance diagrams was investigated by the use of literature and experimental values for the different parameters, as presented in Table 2. For a thin Li_3N film, it has been assumed that the fraction $(1-\Theta)$ of the surface area covered by the liquid phase, and the number n of pores per unit area are considerably lower than those characteristic of the thick porous Li_3N film. It has also been assumed that the conductivity of the solid phase is given by the transcrystalline and intercrystalline conductivities of Li_3N sinters. The impedance of the pore base is assumed to be the low impedance of the metal/solution interface, while the impedance of the pore wall is the high impedance of an electronic insulator in contact with the solution.

As shown in Figs. 17 and 18, computer-generated impedance diagrams in the complex plane can be obtained which approximate the experimental diagrams. A large dispersion parameter has been used for the intercrystalline impedance to obtain a similar shape over the whole frequency range. An increase of the fraction $(1-\Theta)$ and the number n, which both are related to the porosity of the film, leads to a decrease of the total impedance. Thus, the change of the impedance observed as a function of different factors, such as the immersion time and polarization conditions, can be explained by a change of the surface area of the Li electrode in contact with the organic electrolyte via pores in the Li_3N film.

CONCLUSIONS

1. Formation of lithium nitride by reaction of lithium and nitrogen at ambient temperature results in a microporous film, the porosity of which is related to the decrease of the molar volume during the reaction.

2. The impedance behavior of the film-covered electrode can be interpreted by a porous-film model deduced from a transmission-line model.

3. Changes in the impedance behavior of the lithium/lithium nitride electrode with immersion time, anodic, and cathodic polarizations have been attributed to the slow filling of the micropores in the lithium nitride film and reaction of exposed lithium

with the solution.

4. Despite its low thermodynamic potential, lithium nitride shows no evidence of decomposition in a propylene carbonate-based solution even under anodic polarization.

5. Lithium nitride formed by reaction of Li with N_2 is not suitable as a solid-electrolyte interphase between lithium and an organic electrolyte because contact of the unprotected metal with solution results in decomposition reactions during cycling.

ACKNOWLEDGMENT

REFERENCES

1. K.M. Abraham and S.B. Brummer, in Ambient Temperature Lithium Batteries, edited by J.P. Gabano, Academic Press, London, 1983, p. 371.

2. J.G. Thevenin and R.H. Muller, Lawrence Berkeley Laboratory Report, LBL-20660 (1986).

3. A. Rabenau, Solid State Ionics 6 (1982) 277.

4. U. Von Alpen, A. Rabenau, and G.H. Talat. Appl. Phys. Lett. 30 (1977) 621.

5. B.A. Boukamp and R.A. Huggins, Mat. Res. Bull. 13 (1978) 23.

6. F.J. Schwager and R.H. Muller, Electrochem. Soc. Meeting, Detroit, MI, Oct. 17-21, 1982, Ext. Abs. No. 295.

7. K.S. Cole and R.H. Cole, J. Chem. Phys. 9 (1941) 341.

8. R. de Levie, in Advances in Electrochemistry and Electrochemical Engineering, Vol. 6 edited by P. Delahay and C.W. Tobias, Wiley Interscience, New York, 1967, p. 329.

9. J.R. Park and D.D. MacDonald, Corrosion Science 23 (1983) 295.

10. R.W.G. Wyckoff, Crystal Structures, Vol. 1 Robert Krieger Publishing Co., Melbourne, Florida, 1982, p. 16.

11. A.F. Wells, Structural Inorganic Chemistry, Oxford University Press, 1975, p. 241.

12. R.M. Yonco, E. Valeckis, and V.A. Maroni, J. Nucl. Mat. 57 (1975) 317.

13. A. Bonomi, M. Hadate, and C. Gentaz, J. Electrochem. Soc. 124 (1977) 982.

Table 1. Selected Properties of Lithium Nitride.

	single crystal[4]	sinter[5]	present work
Conductivity, $\Omega^{-1}cm^{-1}$	$\sigma_{//} = 1.2 \times 10^{-3}$	$\sigma_t = 6 \times 10^{-4}$	$\sigma_t = 3 \times 10^{-4}$
	$\sigma_{\perp} = 1 \times 10^{-5}$	$\sigma_i = 3 \times 10^{-6}$	$\sigma_i = 6 \times 10^{-5}$
Density, g/cm^3	1.29	1.26	porous 0.97
			compact 1.22

Table 2. Values for the parameters used in the transmission line model.

Parameter	Value
Fraction of the electrode surface covered by the solid phase.	$\Theta = 0.95$
Number of pores per unit area filled by the liquid phase.	$n = 10^{+4}$
Thickness of the porous electrode.	$L = 10^{-2}$ cm
Electrolyte resistance.	$R_\Omega = 15 \ \Omega \ cm^2$
Resistance of the liquid phase (for a thickness of 0.01 cm)	$RL = 2 \ \Omega \ cm^2$

Impedance of the solid phase
(for a thickness of 0.01 cm)

Transcrystalline impedance ZT

Intercrystalline impedance ZI

$ZS \begin{cases} ZT & \begin{cases} RT = 15 \ \Omega cm^2 \\ CT = 1 \ nF/cm^2 \end{cases} \\ ZI & \begin{cases} RI = 3000 \ \Omega cm^2 \\ CI = 1 \ nF/cm^2 \end{cases} \end{cases}$

Impedance of the pore base.	ZB	$\begin{cases} RB = 10 \ \Omega cm^2 \\ CB = 10 \ \mu F/cm^2 \end{cases}$
Impedance of the pore wall.	ZP	$\begin{cases} RP = 5000 \ \Omega . cm^2 \\ CP = 25 \ \mu F/cm^2 \end{cases}$

FIGURE CAPTIONS

Fig. 1. Model of a compact lithium-nitride film. (a) schematic

view of a compact polycrystalline material covering a

metal electrode; (b) equivalent electrical circuit;

(c) impedance diagram in the complex plane.

Fig. 2. Model of a porous lithium-nitride film. (a) schematic

view of a porous polycrystalline material of

thickness L covering a metal electrode; (b) equivalent

electrical circuit; (c) impedance diagram in the

complex plane.

Fig. 3. SEM of the surface of a thin lithium nitride film (0.01

cm thick) formed by 20 minutes of exposure of a lithium

electrode to a pure nitrogen atmosphere. Cutting direction

from upper right to lower left. Scale line 28 μ m.

Fig. 4. SEM of the cross-section of a thin lithium nitride film

showing its minimum thickness of about 0.01 cm in the

center of the disc of 0.2 cm diameter. Free surface

faces down, film formed by 20 minutes of exposure of

lithium to nitrogen. Scale line 66.7 μ m, arrows

indicate 100 μ m film thickness.

Fig. 5. SEM of the surface of a thick lithium nitride film (0.7 cm

thick) formed by 1 hour of exposure of a lithium electrode

to a pure nitrogen atmosphere. Formation of cracks and

holes in the center of the film. Scale line 91.7 μ m.

Fig. 6. Mercury porosimetry of three separate lithium nitride samples

0.7 cm thick and 0.3 cm in diameter. Cumulative

pore-volume as a function of applied mercury pressure or

pore radium.

Fig. 7. Mercury porosimetry of lithium nitride. Differential

pore-volume density as a function of pore radius, derived

from Fig. 6.

Fig. 8. Influence of immersion time in the organic electrolyte

on the open-circuit potential of a Li/Li_3N electrode.

Time of exposure of lithium to nitrogen: (a) 20 min.;

(b) 30 min.; (c) 40 min.

Fig. 9. Influence of cathodic polarization on the

potential of the Li/Li_3N electrode.

Film formed by 30 min. exposure of Li to N_2.

(a) open-circuit potential after immersion in solution;

(b) potential during cathodic polarization (current

density 0.5 mA/cm^2); (c) open-circuit potential

following cathodic deposition (charge density 0.5 C/cm^2).

Fig. 10. Influence of anodic polarization on the potential of the

Li/Li_3N electrode. Film formed by 30 min. exposure of

Li to N_2. (a) open-circuit potential after

immersion in solution; (b) potential during anodic

polarization (current density 0.5 mA/cm^2);

(c) open-circuit potential following anodic dissolution

(charge density 0.5 C/cm^2).

Fig. 11. Influence of thickness and time of immersion of the Li/Li N electrode on impedance diagram at the open-circuit potential. Time of exposure of lithium to nitrogen: (a) 20 min.; (b) 30 min.; (c) 40 min.

Fig. 12. Influence of immersion time in the solution of the Li/Li$_3$N electrode on the impedance diagram at the open-circuit potential. Film formed by 20 min. exposure of Li to N$_2$. (a) reference (initial) diagram; (b) after 24 hrs.; (c) after 48 hrs.

Fig. 13. Influence of cathodic polarization of the Li/Li$_3$N electrode on the impedance diagram. Film formed by 30 min. exposure of Li to N$_2$. Current density of -0.25 mA/cm^2. (a) reference diagram; (b) after charge density of 1 C/cm^2; (c) after charge density of 5 C/cm^2.

Fig. 14. Influence of anodic polarization of the Li/Li$_3$N electrode on the impedance diagram. Film formed by 30 min. exposure of Li to N$_2$. Current density of +0.25 mA/cm^2. (a) reference diagram; (b) after discharge density of 1 C/cm^2;(c) after discharge density of 5 C/cm^2.

Fig. 15. Influence of a single deposition/dissolution cycle of the Li/Li$_3$N electrode on the impedance diagram. Film formed by 30 min. exposure of Li to N$_2$. Current density of 0.5 mA/cm^2 and charge density of 1 C/cm^2. (a) reference diagram; (b) after cathodic deposition; (c) after anodic dissolution.

Fig. 16. Influence of cycling of the Li/Li$_3$N electrode on the
impedance diagram. Film formed by 20 min. exposure

of Li to N$_2$. Reference diagram before cycling is given

in Fig. 12c. Current density of 0.5 mA/cm^2 and charge

density of 1 C/cm^2.

(a) 1st cathodic deposition; (b) 1st anodic dissolution;

(c) 2nd cathodic deposition; (d) 2nd anodic dissolution;

(e) 5th cathodic deposition; (f) 5th anodic dissolution.

Fig. 17. Computer-generated impedance diagram based on the porous-
film model (transmission-line model). Main parameters are
given in Table 2. Influence of the fraction Θ of surface
area covered by the solid phase. (a)Θ = 0.95; (b)Θ =
0.925; (c) Θ = 0.90.

Fig. 18. Computer-generated impedance diagram based on the porous-
film model (transmission-line model). Main parameters are
given in Table 2. Influence of the number n of filled
micropores per unit area. (a) n = 10 ; (b) n = 10 ;
(c) = 10 .
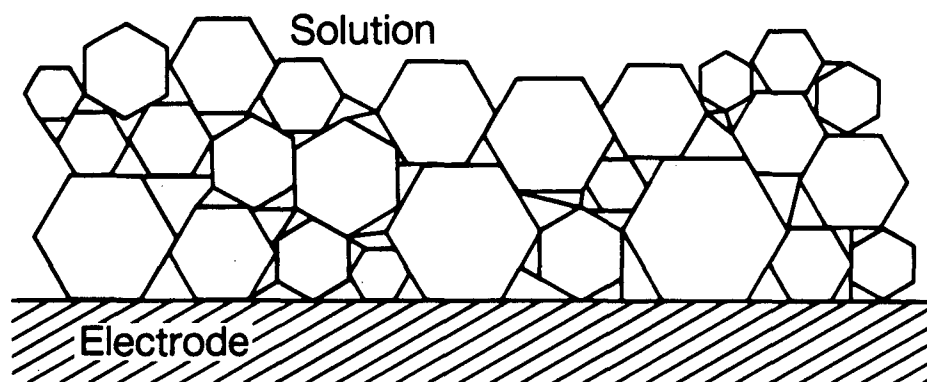
(a)

Solution

Electrode

(b)

C_t

C_i

$[\alpha_t]$

$[\alpha_i]$

R_Ω

R_t

R_i

(c)

Z'' $\omega \rightarrow \infty$

R_Ω

$\omega \rightarrow 0$

0    $\alpha_t \Pi/2$ $\alpha_i \Pi/2$

$R_\Omega + R_t$ Z' $R_\Omega + R_t + R_i$

XBL 861-9724

Fig. 1

(a)

Solution

Electrode

(b)

$$Z_s \frac{dx}{L}$$ // $$Z_s \frac{dx}{L}$$ $$Z_s \frac{dx}{L}$$

$$\frac{1}{Z_p} \cdot \frac{dx}{L}$$ $$\frac{1}{Z_p} \cdot \frac{dx}{L}$$ $$\frac{1}{Z_p} \cdot \frac{dx}{L}$$ $$Z_b$$

$$R_\Omega$$ $$R_l \frac{dx}{L}$$ // $$R_l \frac{dx}{L}$$ $$R_l \frac{dx}{L}$$

(c)

$$Z''$$ $$\omega \rightarrow \infty$$

$$R_\Omega$$

$$\omega \rightarrow 0$$

0    $$R_\Omega$$ $$R_\Omega + R_T$$

$$Z'$$

XBL 861-9723

Fig. 2

20KV   357X   28.0M 0002

XBB 850-9092

Fig. 3

20KV   150X ‾‾‾‾‾‾ 66.7µ 0007

XBB 850-9093

Fig. 4

20KV   109X   91.7M 0001
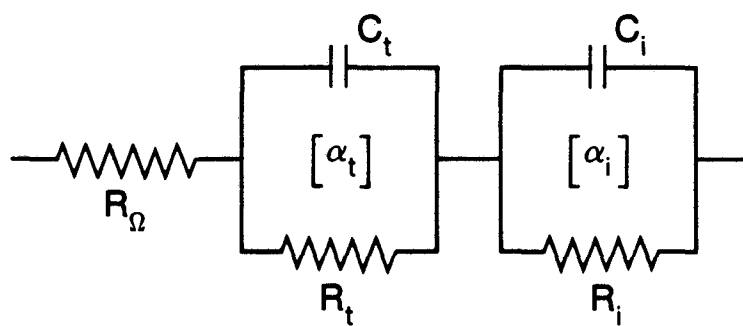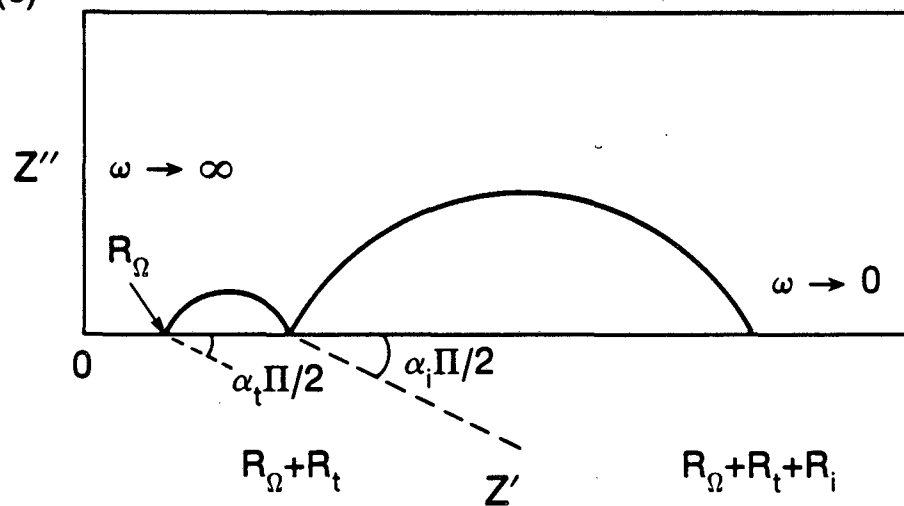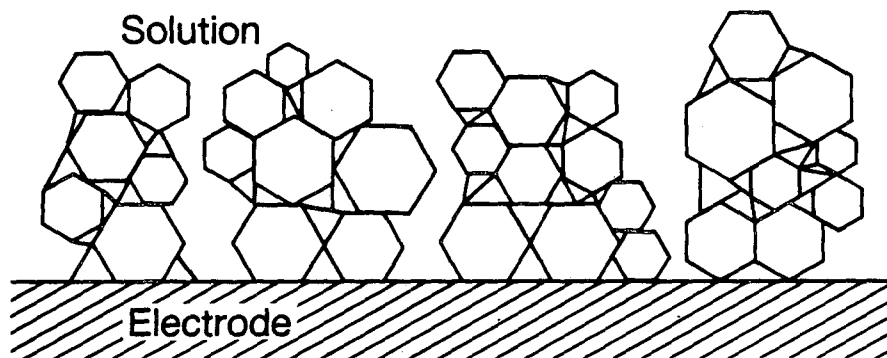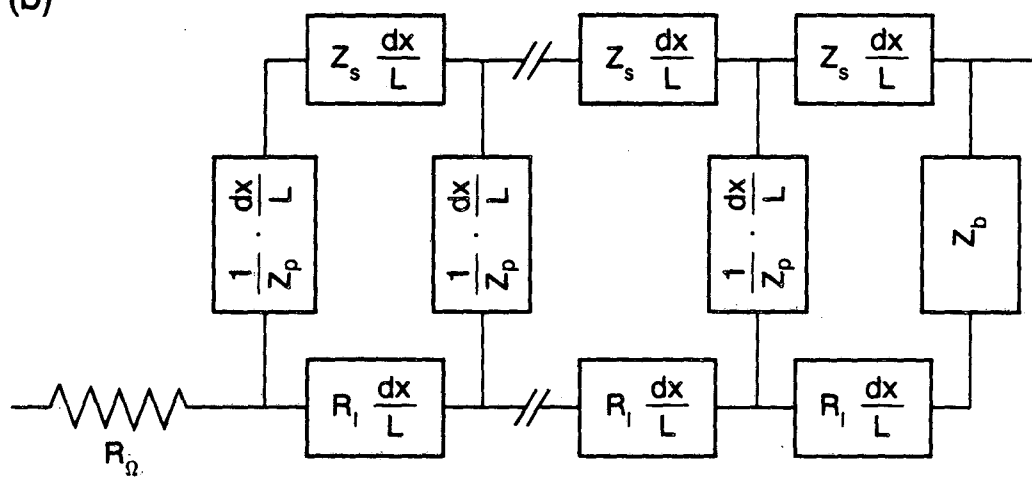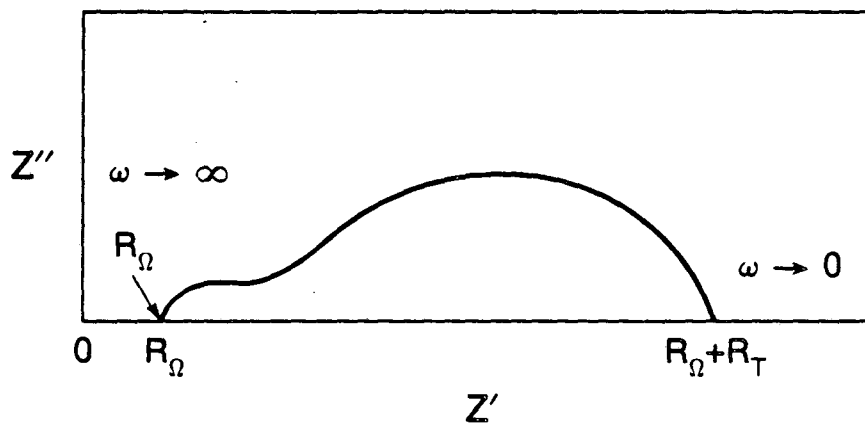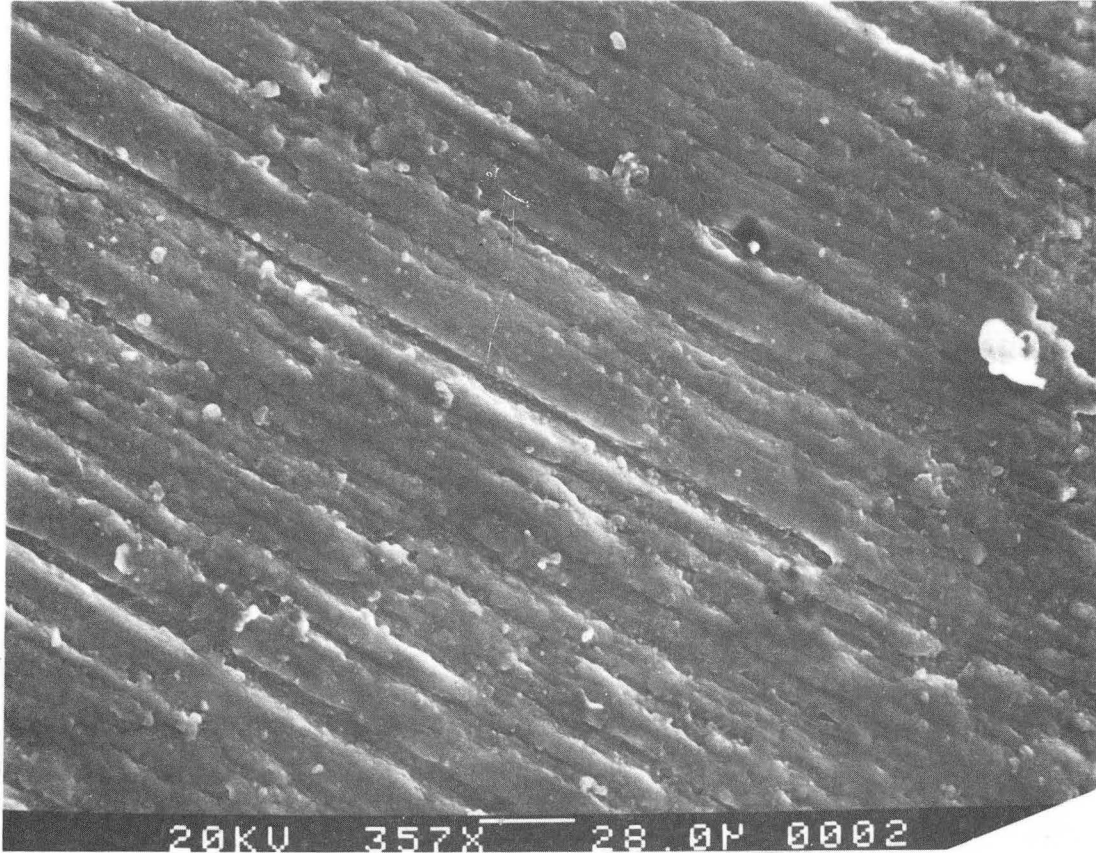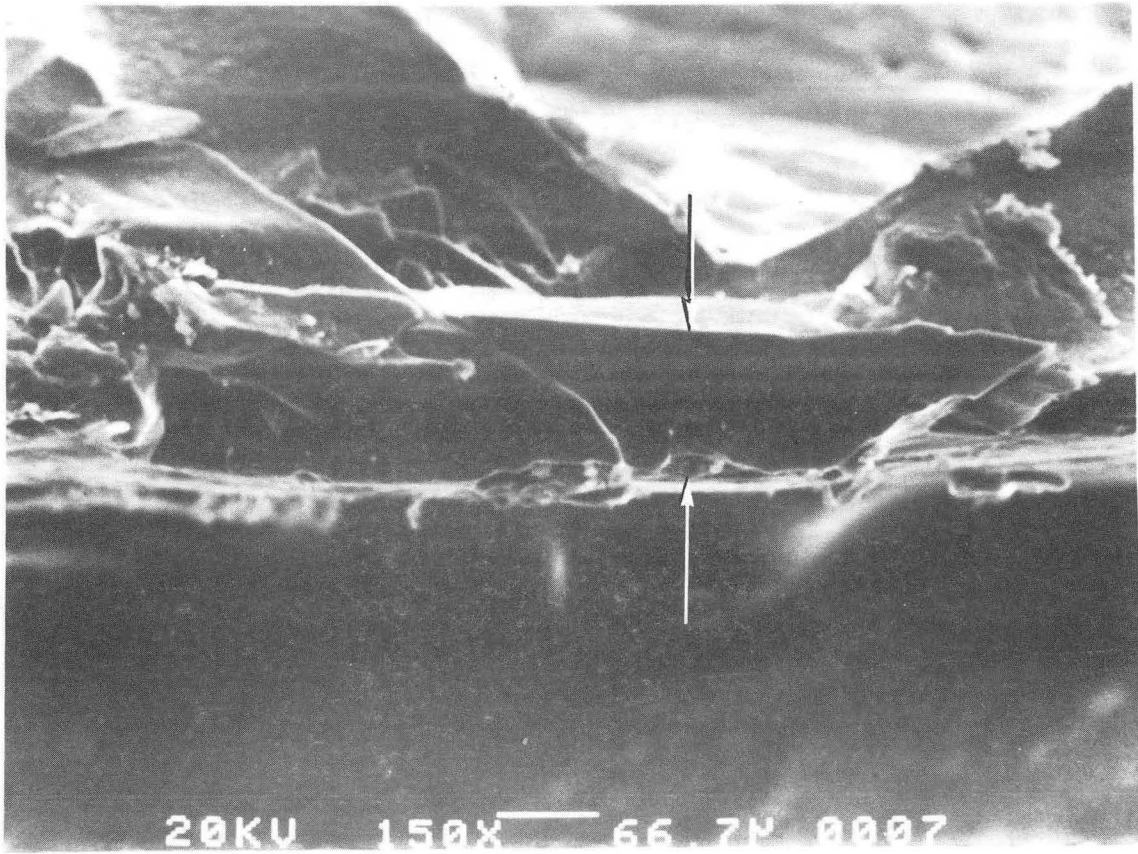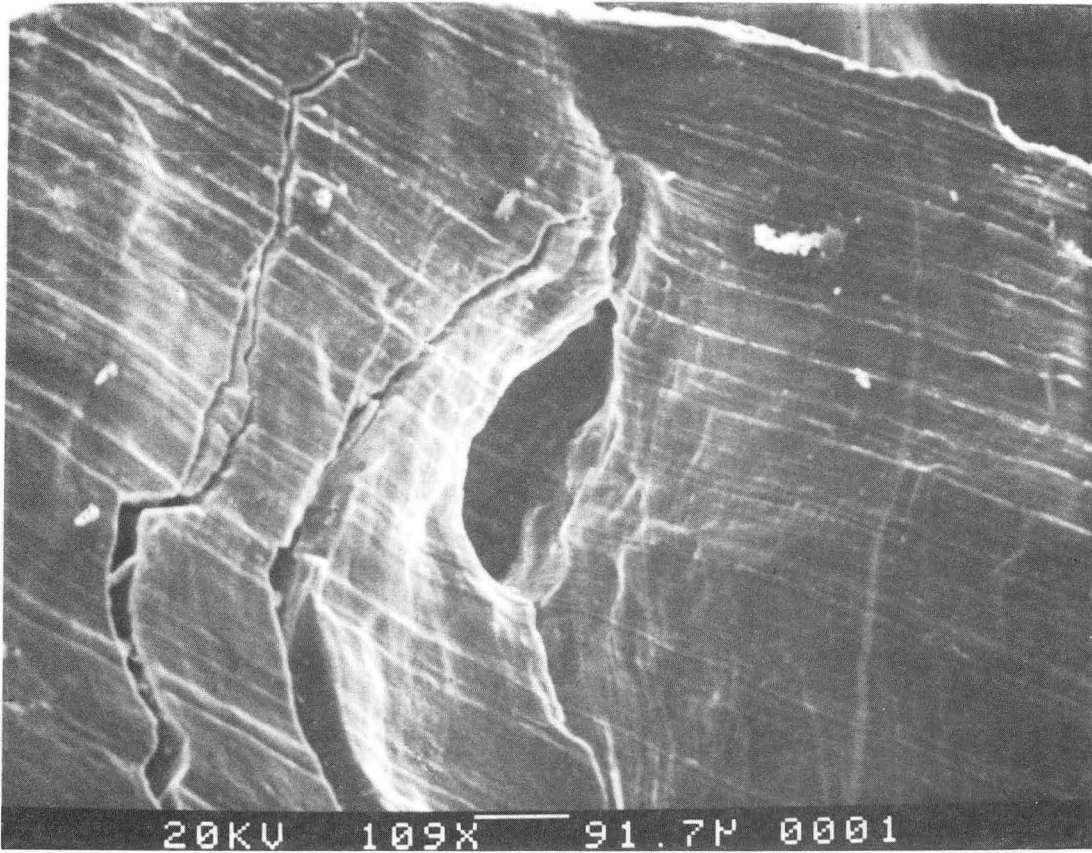
XBB 850-9094

Fig. 5

XBL 8511-11440

Fig. 6

$$D_v(R) = P\ dV/R\ dP$$

Fig. 7

XBL 8511-11442

XBL 861-6078

Fig. 8

Fig. 9

XBL 861-6080

Fig. 10

XBL 861-6076

Fig. 11

XBL 861-9105

Fig. 12

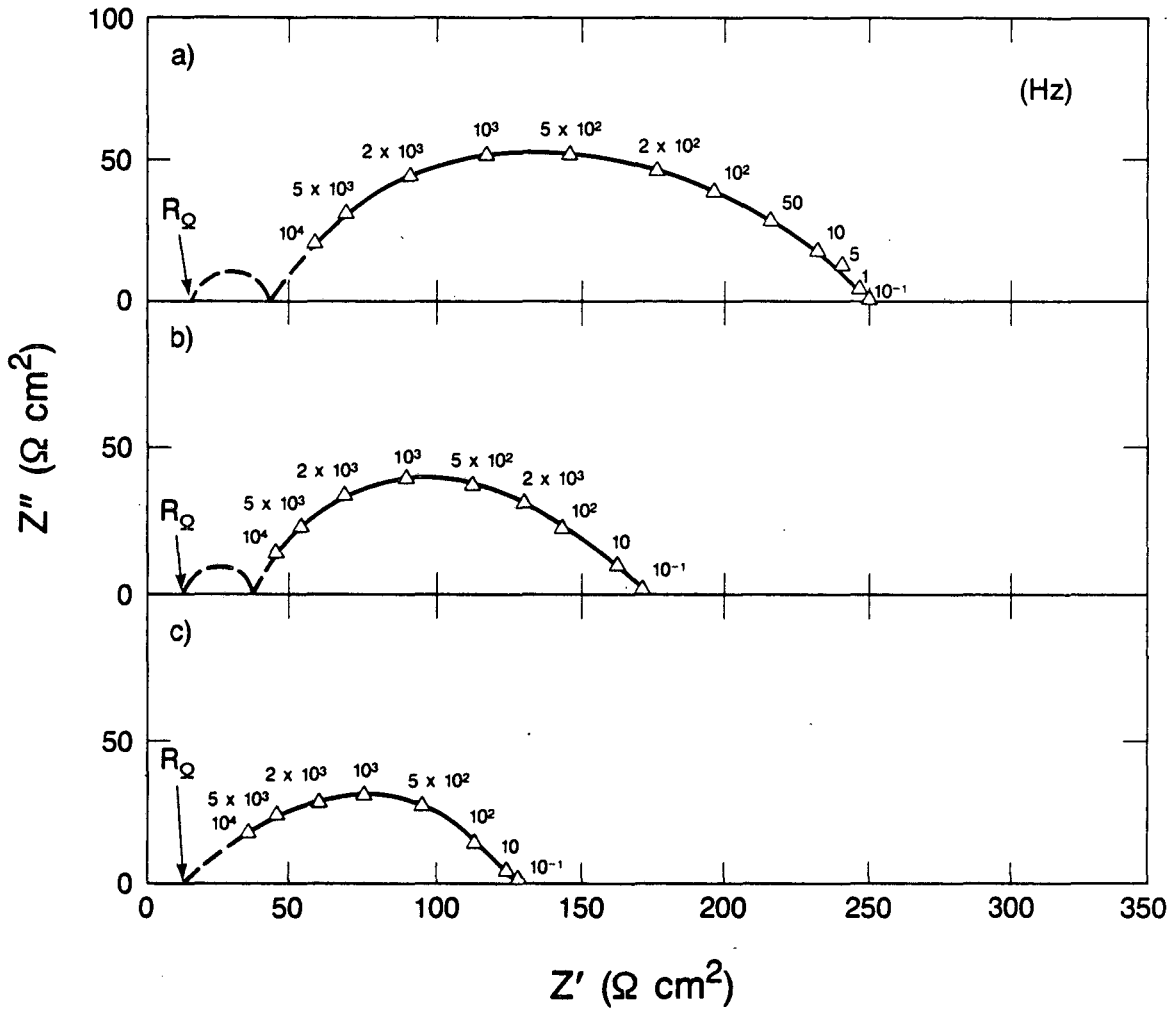XBL 861-6048

Fig. 13

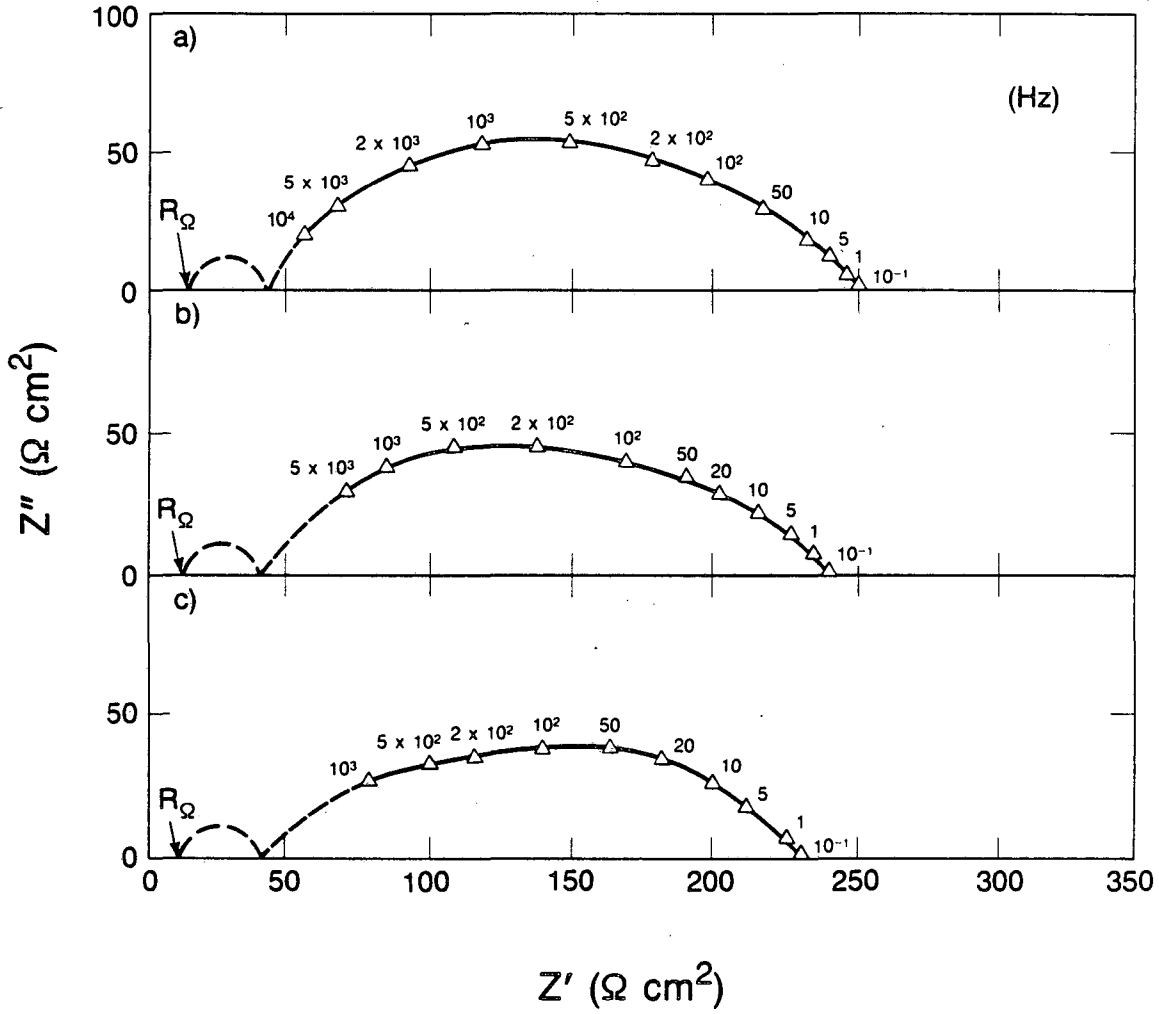XBL 861-6049

Fig. 14

XBL 861-6041

Fig. 15

XBL 861-6045

Fig. 16

XBL 861-6081

Fig. 17

XBL 861-6040

Fig. 18

XBL 861-6115